Mechanisms Regulating Deep Moist Convection and Sea-surface Temperatures of the Tropics

Y. C. Sud, G. K. Walker* and
K. M. Lau

October 8, 1998

Climate and Radiation Branch
Laboratory for Atmospheres
NASA/Goddard Space Flight Center
Greenbelt, MD 20771

(Submitted as a NOTE to GRL)

*General Sciences Corporation, Laurel, Maryland

ABSTRACT

Despite numerous previous studies, two relationships between deep convection and the sea-surface temperature (SST) of the tropics remain unclear. The first is the cause for the sudden emergence of deep convection at about 28°C SST, and the second is its proximity to the highest observed SST of about 30°C. Our analysis provides a rational explanation for both by utilizing the Improved Meteorological (IMET) buoy data together with radar rainfall retrievals and atmospheric soundings provided by the Tropical Ocean Global Atmosphere Coupled Ocean-Atmosphere Response Experiment (TOGA-COARE). The explanation relies on the basic principles of moist convection as enunciated in the Arakawa-Schubert cumulus parameterization. Our analysis shows that an SST range of 28-29°C is necessary for "charging" the atmospheric boundary layer with sufficient moist static energy that can enable the towering convection to reach up to the 200 hPa level.

In the IMET buoy data, the changes in surface energy fluxes associated with different rainfall amounts show that the deep convection not only reduces the solar flux into the ocean with a thick cloud cover, but it also generates downdrafts which bring significantly cooler and drier air into the boundary-layer thereby augmenting oceanic cooling by increased sensible and latent heat fluxes. In this way, the ocean seasaws between a net energy absorber for non-raining and a net energy supplier for deep-convective raining conditions. These processes produce a thermostat-like control of the SST. The data also shows that convection over the warm pool is modulated by dynamical influences of large-scale circulation embodying tropical easterly waves (with a 5-day period) and MJOs (with 40-day period); however, the quasi-permanent feature of the vertical profile of moist static energy, which is primarily maintained by the large-scale circulation and therodynamical forcings, is vital for both the 28°C SST for deep convection and its upper limit at about 30°C.

1. Introduction

A discernible relationship between the sea-surface temperature (SST) and the depth or intensity of overlying moist convection (MC) has been pointed out in a large number of previous studies (e.g., Gadgil et al., 1984; Graham and Barnett, 1987; and Zhang, 1993). One key feature of tropical convection is that deep convection emerges at SSTs greater than 28°C. Not only is the association of deep convection to the 28°C SST remains unexplained, but its close proximity to the upper limit of observed SSTs (about 30°C) is an intriguing part of the puzzle. To address the latter problem, several hypotheses have been proposed including the well known thermostat hypothesis of Ramanathan and Collins (1991) and the role of super greenhouse effect of water vapor in reducing the radiative forcing of the oceans (Weaver et al., 1994) while several other scientists have stressed the need to include important effects such as evaporation, large-scale forcing, and vertical motion fields associated with moist convection (e.g., Lau et al., 1994; Waliser and Graham, 1993; Hartmann and Michelson, 1993; Wallace, 1992; Fu et al., 1992). Utilizing the analysis of observations for 1987 and 1988 and satellite retrievals, Bony et. al (1997) examined the inter-relationships among the vertical distribution of water vapor, clouds, large-scale rising motion fields, MC, and local SSTs in the tropics. They identified a correspondence among SSTs, large-scale vertical motion, and MC and argued that the intense convection is, in part, a consequence of organized large-scale vertical motion. In this way, they affirmed the dual role of local and remote forcings in maintaining moist convection in the tropics as has also been inferred by Lau et al. (1996). Both studies found that in certain tropical regions, a sharp increase in moist convection starts at about 26.5°C and reaches a maximum at about 29.5°C. The basic result, in agreement with several others, shows that deep convection over the tropical oceans appears at about 28°C while the observed SST rarely exceeds 30°C.

We must emphasize, however, that the SST thresholds discussed above does not hold good outside of the tropics. For example, strong deep convection often appears in boreal winters over the warm waters of the Gulf stream off the east coast of the United States even when the SSTs

are in the 20^0C range. This indicates that tropical SST and its overlying deep convection must be strongly linked to a persistent, even quasi-stationary, vertical thermodynamical structure of the tropical atmosphere, and that the upper limit of SSTs may be affected by changes in surface energy budget related to moist convection. In this research letter, we will investigate: (i) why does deep tropical convection ensue at about 28^0C SST?; and (ii) how is the upper limit of about 30^0C SSTs maintained in the tropics? We employ the TOGA-COARE data collected in the Intensive Observations Periods (IOP) from IMET buoy (due to Woods Hole Oceanographic Institute, WHOI) -- 01 Nov., 1992 through 28 Feb., 1993 (Weller and Anderson, 1996), and analyzed rainfall estimates from radar reflectivities that are described in Rutledge et al. (1993) and Short et al. (1997). The inferences on the first question are re-evaluated with the ECMWF analysis of observations for one year: 01 Jan. 1989 through 31 Dec. 1989.

2. Deep Convection and 28°C SST.

Let us recapitulate our current understanding of the thermodynamics of moist convective adjustment. According to the classical paradigm of Arakawa and Schubert (1974, hereafter A-S), the cumulus adjustment process is literally driven by the instability of the vertical profile of moist static energy which is maintained by large scale circulation plus surface fluxes. As shown in Fig. 1, cumulus clouds emerge near the top of atmospheric boundary layer (ABL) whenever the ABL-airmass becomes convectively unstable and is moist enough for the release of latent heat in ascent. Since cloud bases usually appear at or just above the ABL, one can safely assume that the moist static energy at the ABL top is roughly equal to the moist-static energy of the convective cloud, $\mathbf{h_{cloud}}$ (= $c_pT + gz + Lq$), at its base. The corresponding ambient saturation moist static energy, $\mathbf{h^*}$ (= $c_pT + gz + Lq^*$) is computed to determine if an ascending cloud in its surroundings is buoyant or not. The variables represent specific heat of air, c_p; temperature, T; acceleration due to gravity, g; height above sea level, z; latent heat of evaporation, L; and the ambient (saturation) specific humidity, q (q^*). Naturally, cumulus clouds in ascent conserve $\mathbf{h_{cloud}}$ and detrain as soon as $\mathbf{h_{cloud} = h^*}$. However, by entraining ambient air, clouds suffer a

reduction in their moist static energy. This is schematically shown by different curved paths (drawn dotted) for several arbitrarily chosen cloud entrainment rates, Fig. 1. The cloudy air parcels, emerging out of the convectively unstable ABL, organize themselves into convective ensembles of different shapes and sizes and naturally ascend to seek the level of neutral buoyancy. Smaller (larger) clouds entrain more (less) and consequently detrain at a lower (higher) level. Sud et al. (1995, 1993) used the above construct to explain the response of rainfall to biospheric processes. They noted that the key results of almost all GCM simulation studies invoking changes in land surface albedo, evapotranspiration, and surface roughness could be explained by relating the ABL (modified by these processes) to its influence on moist convection. In this work, we adopt the same methodology to explain the observed relationship between deep-convection and tropical SST. Using the saturation moist static energy at different cloud-detrainment levels, we can determine the minimum SST necessary to supplant the boundary-layer and the cloud base atop with the essential moist static energy. We assume that the maximum $\mathbf{h_{cloud}}$ is controlled by SST, while $\mathbf{h^*_{top}}$ is a function of a multitude of physical and dynamical interactions that must be determined from data.

According to Figure 1, a cloud-parcel (without entrainment) could reach a targeted pressure level if and only if its initial moist static energy $\mathbf{h_{cloud_i}}$ is greater than the ambient $\mathbf{h^*_{top}}$ at that level. The SST needed to support $\mathbf{h_{cloud_i}}$ can be deduced by requiring that the SST, at saturation, is produces $\mathbf{h_{cloud_i}}$. Figures 2a and b show several isolines of saturation moist static energy at four selected pressure levels --1000 (Sea-surface), 850 (low level), 500 (mid level), and 200 (high level) hPa as a function of S/c_p -273.16 (=**S**)where S is dry-Static Energy. If we adopt 90% relative humidity and 950 hPa for cloud base, it yields an additional isoline for the cloud base moist static energy (shown by a thin curve). The small boxes riding on the isolines represent the observed **S**-range, inferred from $\mathbf{S}_{mean} \pm$ 2-standard deviation of **S** at the three selected pressure levels: 850, 500, and 200 hPa. The TOGA-COARE data for the entire IOP at these pressure levels is shown in Fig. 2a, and the ECMWF 1989 analysis for all tropics is plotted

in Fig. 2b. The tropical environment has a truly narrow range of observed dry static energies expressed by S/c_p- 273.16; this scenario is well maintained at all pressure levels including those not shown in the figures (to avoid cluttering). Relatively, the range of **S** for all tropical regions is little broader than that of the warm pool region but both of them are significantly smaller than extratropical regions such as Gulf Stream (analyzed but not shown). By drawing horizontal lines from the upper and lower values of $\mathbf{h}^*_{top}$ to the isolines of moist static energy at the cloud base (thin line), we infer the potential temperature at the cloud base which must equals SST under ideal conditions. The SST range is projected on the abscissa and for convection reaching 200 hPa, it is about 26-27°C.

The above procedure yields the minimum SST that under ideal conditions would barely enable the ABL air-mass to reach the top with the moist static energy = $\mathbf{h}^*_{top}$. However, the A-S scheme includes additional allowances for the real atmosphere. It allows for reduction of moist static energy by cloud-entrainment, and the need for generating the minimum cloud work function invoked by critical cloud work function (CCWF) which is a measure of convective instability. In essence, $\mathbf{h}_{\mathbf{cloud}_i}$ at the cloud base must be larger than the ambient $\mathbf{h}^*_{top}$. However, because deep clouds can be surrounded by shallower clouds, the A-S scheme allows the possibility of very deep clouds with minimal entrainment. While in ascent, clouds accelerate due to buoyancy whose generation depends upon the vertical profile of $\mathbf{h}^*$. If $\mathbf{h}_{\mathbf{cloud}_i}$ exceeds $\mathbf{h}^*_{top}$ by CCWF, convection is guranteed. Hence we assume $\mathbf{h}_{\mathbf{cloud}_i} = \mathbf{h}^*_{top}$ + CCWF. For a cloud traversing from 950 hPa to 200 hPa, it is roughly 1.8 kJ/kg (Sud et al., 1991). In addition there is always a difference in the saturation moist static energy at the sea-surface, $\mathbf{h}_{SST}$ and $\mathbf{h}_{\mathbf{cloud}_i}$ at 950 hPa; we call it Δh_{ABL}.= $h^*_A - h_B$ in Fig. 1. In the IMET data, Δh_{ABL} is about 7.80 kJ/kg. This allowance yield: $\mathbf{h}_{SST} = \mathbf{h}_{\mathbf{cloud}_i} + \Delta h_{ABL}$ (= $\mathbf{h}^*_{top}$ + CCWF + Δh_{ABL}). These corrections shift the horizontal lines of $\mathbf{h}^*_{top}$ upward to yield somewhat higher SSTs as depicted in the revised panels of Figs 2a and 2b (shown on the left). Thus, for convection to reach 200 hPa, the inferred SST range becomes 28-29°C which is well supported by observations (Lau et al., 1996). Another

inferences is that cloud detrainment at 500 hPa (mid-level) need the least $\mathbf{h_{cloud_i}}$ but since all clouds must first pass through the 850 hPa, they emerge with larger than the minimum $\mathbf{h_{cloud_i}}$ for mid-level clouds. Naturally such clouds are too buoyant to detrain at the 500 hPa level. This reveals why there is preponderance of shallow and deep clouds in the tropics, a fact that has been variously noted and explained before. A similar analysis with the ECMWF data for the entire tropical oceans, Fig. 2b, shows that our inferences about deep convection-SST relationships remain robust.

3. Deep Convection as a Thermostat

Because of the proximity of 28°C SST (for deep convection) to the maximum observed SST of 30°C, it is highly plausible that the deep convection has a limiting influence on the SST beneath. We evaluate the thermostat hypothesis due to Ramanathan and Collins (1991) by examining the influence of deep convection on the net energy flux into the ocean using the IMET buoy data. Figure 3 shows the evolution of SST anomaly with time. One notes a 5-7 day time-scale with positive (negative) net energy into the oceans for non raining (raining) conditions. The fluctuations are superposed on a much slower time scale of about 40 days. The horizontal lines on Fig. 3(b) represent the time-average net radiation into the ocean; it is about 135 W m^{-2}. Of this, only 15 W m^{-2} is the energy advected out of the region by oceanic circulation. The rest is balanced by sensible and latent fluxes. Being the warmest region of the ocean, we expect the flux divergence to be positive. Nevertheless, the major energy balance is between net radiation and surface fluxes of heat and moisture, while the SST adjustment cycles concur with the time periods of easterly waves and MJOs. Figure 4 shows a sample analysis for 3 months of data; it reveals that the upward net energy flux from the ocean is associated with high precipitation (shown green) and cloudiness. Evidently, intensely raining clouds create conditions for reduced net radiation flux into the ocean, the so called "cloud shielding effect of solar energy", but this is accompanied by an equally large increase in surface fluxes of sensible and latent heat. In a few cases, precipitation does not affect the net radiation much; those are primarily nighttime episodes

with clouds advecting out of range or dissipating by day-break. It is interesting that the periods with positive net energy into the ocean are longer and generally rainfree. Figure 5, shows that the moist static energy binned by rainfall amount. Quite interestingly, higher rainfall leads to lower moist static energy. Since evaporation of falling rain can not change the moist static energy of the airmass, a reasonable explanation is that subsidence and or downdrafts are causing it. In the top panel of Fig. 5, we note a steady moist static energy of 349.0 ± 0.5 kJ/kg before the precipitation; it sharply reduces by 2 to 6 kJ/kg after the precipitation event. This reflects a reduction in temperature of 1.5°C or less. Recognizing that downdrafts occur over a much smaller region as compared to the data domain while our statistics can be contaminated by neighboring precipitation events, the role of downdrafts in producing local cooling is captured only partially. Saxen and Rutledge (1998) noted peak downdraft cooling magnitudes of 4.0°C in agreement with several other insitu observations. We emphasize that the downdraft cooling and drying has a critical role in enhancing the surface fluxes and promoting oceanic cooling in association with deep convection. The altered net surface energy fluxes have a life cycle of several hours particularly for large rainfall episodes. Indeed the net radiation continues to be positive for several hours before the raining period but sometimes it may be reduced by cloud build up making the net energy flux into the ocean negative.

Figure 6 shows that the energy lost by the sea-surface through sensible and latent fluxes. It increase from about 100 W m^{-2} for the no precipitation cases to almost 190 W m^{-2} at about 4-5 mm h^{-1} precipitation rate. In their analysis, Saxen and Rutledge (1998) note sensible and latent fluxes beneath the downdrafts peaking at 60 W m^{-2} and 250 W m^{-2} respectively; this is cleaqrly a consequence of drying, cooling, and wind-bursts. Time-lag variations reveal that the increase in surface fluxes can occur within an hour of the precipitation but its full recovery can take up to 10 hours. Since it may be difficult to have a 10h period precipitation free period, the statistics on longer time lag or lead may again be contaminated. The net radiation plot, Fig. 6, shows a similar picture for positive lag but the picture for negative lag is puzzling. For up to 5 mm h^{-1}

precipitation, the net radiation at 10h lead is about the same as at 2h lag with a maximum at about 3h lead. This would be related to the cloudiness variation on those time scales. At this stage, we are unable to isolate the dynamics of this relationship; regardless, we have discerned the key results which show that cloudiness associated with convection reduces the shortwave influx by about 100 W m^{-2} while the downdraft cooling cause an increase in surface fluxes of about 90 W m^{-2}. The net result is a deficiency of 190 W m^{-2} in the ocean energy flux which causes it to cool. In view of this scenario, we infer that SST may not exceed the inferred temperature limit of about 29°C for deep-moist convection. Why then do we have SST of 30°C or sometimes even 31C? This may have the following explanation: (i) we only used the two standard deviations for the potential temperature aloft to eliminate the outliar in the observations some of which may be real, (ii) the large-scale systems have dynamical modulations involving 5-day and 40-60 day cycles; these reflect in the SST cycles which can produce larger $\mathbf{h}^{*}_{\mathbf{top}}$ in the warming phase, and (iii) the large-scale forcing may produce strong sinking motion that continues to dry the boundary layer allowing hot spots to develop (Waliser, 1996). However, only a few degrees rise in SST, which has the time-scale of a week, may be able to inject enough moist static energy into the ABL to enable it override the influence of normal vagaries of weather and/or remote forcings embodied in the dynamical cycles. Thus, SST can exceed beyond the deep convective cooling limit of 28°C but not much further.

5. Conclusion and Summary

We have used the TOGA-COARE and ECMWF analyses of atmospheric soundings and the IMET buoy data together with radar rainfall estimates at the buoy location to answer two basic questions about the observed relationship between tropical convection and sea-surface temperature (SST). The first relates to the thermodynamic basis for the sudden emergence of deep convection at about 28°C SST, and the second relates to the proximity of this temperature to the maximum observed SST (about 30°C). Employing the concepts and physical basis of moist convection of the Arakawa-Schubert (1974) cumulus scheme, and the observed and/or analyzed

vertical soundings of the tropical atmosphere, we show that an SST range of 28-29°C is required for charging the ABL with sufficient $\mathbf{h_{cloud_i}}$ for supporting deep convection. We note that these results are not valid outside of the tropics and it suffices to reiterate that the role of tropical soundings is critical for this remarkably simple relationship of the tropics.

We also examined the changes in the thermal forcing of the ocean associated with strong moist convection. We find that deep convection largely suppresses the solar flux into the ocean by producing an optically thick cloud cover, while the associated downdrafts bring cooler and drier air into the boundary-layer which, in turn, cause a substantial increase in evaporation and sensible fluxes. Together, the two effects produce a strong cooling of the ocean. Thus, deep convection, which is often associated with intense rainfall, optically thick cloud cover, and downdrafts, is able to tip off the ocean from a net energy receiver (warming phase) to a an energy loser (cooling phase). The results suggests a thermostat-like control of the SST that partially affirm earlier hypotheses of SST regulation by convection; nevertheless, it is intrinsically more complex than the Ramanathan and Collins (1991) thermostat hypothesis in which only radiative effects were recognized. Indeed, the time series also reflects the dynamical influence of large-scale circulation, such as 5 day tropical easterly wave and MJOs, that modulate the SST adjustment process which may in turn influence the upper limit on SST through the large-scale dynamics; nevertheless the quasi-permanent structure of the tropical soundings are vital for the maintaining the narrow temperature range of deep tropical convection. In this way, our analysis provides a simple answer to the coupling between tropical SST and overlying deep convection.

REFERENCES

Arakawa, A. and W. H. Schubert, 1974: Interaction of cumulus cloud ensemble with the large-scale environment, Part I. *J. Atmos. Sci.*, **31**, 674-701.

Bony, S., Y. C. Sud, K.-M. Lau, J. Susskind, and S. Saha, 1997a: Comparison of NASA/DAO and NCEP-NCAR reanalyses over tropical oceans: Atmospheric Hydrology and Radiation. J. Climate, 10, 1441-1462.

Bony, S., K.-M. Lau, and Y. C. Sud, 1997b: Sea surface temperature and large-scale circulation influences on tropical greenhouse effect and cloud radiative forcing. J. Climate, 10, 2055-2077.

Cheng, M.-D., A. Arakawa, 1997: Inclusion of rainwater budget and convective downdrafts in the ARAKAWA-SCHUBERT cumulus parameterization, Jour. Atmos. Sci. (In Press).

Gadgil, S., P. V. Joseph, and N. V. Joshi, 1984: Ocean-atmosphere coupling over the monsoon regions. Nature, 312, 141-143.

Fu, R., A. D. DelGenio, W. B. Rossow and T. Liu, 1992: Cirrus cloud thermostat tested using satellite data. Nature, 358, 394-397.

Hartmann, D. L., and M. L. Michelsen, 1993: Large-scale effects on the regulation of tropical sea-surface temperature. J. Climate, 6, 2049-2062.

Graham, N. E., and T. P. Barnett, 1987: Observations of sea-surface temperature and convection over tropical oceans. Science, 238, 657-659.

Lau, K.-M., C.-H. Sui, M.-D. Chou, W.-K. Tao, 1994: An inquiry into the cirrus thermostat effect of tropical sea-surface temperature, Geophys. Res. letters, 21, 1157-1160.

Lau, K.-M., H.-T. Wu, and S. Bony, 1996: The role of large scale atmospheric circulation in the relationship between tropical convection and sea-surface temperature, J. Climate, 10, 381-392.

Ramanathan, V., and W. Collins, 1991: Thermodynamic regulation of oceanic warming by cirrus clouds deduced from 1987 El Nino, Nature, 351, 27-32.

Rutledge, S. A., R. Cifelli, c. Demott, W. Peterson, T. Rickenbach, J. Lutz, R. Bowie, M. Strong, and E. Williams, 1993: The shipboard deployment of MIT C-band radar during TOGA COARE. @6 AMS Conference on Radar Meteorology, Norman, OK 371-373.

Saxen, T. R., and S. A. Rutledge, 1998: Surface Fluxes and Boundary-layer recovery in TOGA COARE: Sensitivity to convective organizations, Jour Atmos Sci., (in Press).

Short, D.A., P. A. Kucera, B. S. Ferrier, J. C. Gerlach, S. A. Rutledge, and O. Thiele, 1997: Shipboard radar rainfall patterns within the TOGA COARE IFA. Bull. Amer. Meteor. Soc., 78, 2817-2836.

Sud, Y. C., W. C. Chao, and G. K. Walker, 1991: Contribution to the implementation of Arakawa-Schubert cumulus Parameterization in the GLA GCM. *J. Atmos. Sci.*, **48**, 1573-1586.

Sud, Y. C., W. C. Chao, and G. K. Walker, 1993: Dependence of rainfall on vegetation; theoretical considerations, simulation experiments, observations, and inferences from simulated atmospheric soundings. J. Arid Enviorn., 25, 5-18.

Sud, Y. C., K.-M. Lau, G. K. Walker, and J.-H. Kim, 1995: Understanding biosphere precipitation relationship, theory, model simulations, and logical inferences, Mausam, 46, 1-14

Waliser, D. E., 1996: Formation and limiting mechanisms for veryhigh sea-surface temperatures: Linking the dynamics and thermodynamics, J. Climate, 9, 161-188.

Waliser, D. E., and N. E. Graham, 1993: Convective cloud system and warm pool sea-surface temperature: coupled interaction and self regulation,m. J. Geophys. Res., 98, 12881-12893.

Wallace, J. M., 1992: Effect of deep convection on regulating the tropical sea-surface temperature, Nature, 357, 230-231.

Weaver, C., W. Collins, and H. Grassl, 1994: Relationship between clear-sky atmospheric greenhouse effect and deep convection during the Central Eqatorial Pacific experiment: model calculations and satellite observations. J. Geophys. Res., 99, 25891-25901.

Weller, R. A., and S. P. Anderson, 1996: Surface meteorology and air-sea surface fluxes in the western equatorial warm pool during the TOGA coupled ocean-atmosphere Response Experiment. J. Climate, 9, 1959-1990.

Zhang, C, 1993: Large scale variability of atmospheric deep convection in relation to sea-surface temperature in the tropics. J. Climate, 6, 1898-1913.

Figure Legends

Fig. 1. Classical picture of moist static energy profiles for moist convection adapted from the Arakawa-Schubert (1974) scheme of moist convection. The h (h*) curves are for actual (saturation) moist static energies of the observed GATE-Phase III soundings. Point B represents the moist static energy at the cloud base whereas points B* (A) are the saturation moist static energies at the cloud base (surface). $\Delta h_{ABL} = h_A - h_B$

Fig. 2. A complex plot showing (i) four lines for saturation moist static energy (kJ/kg) versus potential temperature (S/c_p) in °C; (ii) one line for cloud base moist static energy (kJ/kg) assuming 90% RH and 950 hPa pressure; (iii) riders for observed S/c_p with ± 2 standard deviations of S/c_p; and (iv) left panels with CCWF $+\Delta_{PBL}$ corrections to h* (see Text). Top (bottom) panels represent calculations for TOGA-COARE (ECMWF, 1989) analysis of daily data.

Fig. 3 For the IMET buoy data collected in the TOGA-COARE IOP periods, 24h running means of (a) SST anomalies (°C); net energy fluxes into the ocean (W m^{-2}).

Fig. 4 A composite plot of hourly precipitation (green) in mm h^{-1} and 24h running mean of surface fluxes (W m^{-2}) with red (blue) shades for positive (negative) values.

Fig. 5 Moist static energy in kJ/kg (top) and Net thermal forcing of the ocean (W m^{-2}) (bottom). The data was binned into equal sample sizes while lag or lead were used to collocate values at the same locations.

Fig. 6. Same as Figure 5 except for latent plus sensible fluxes (top) and net radiation absorbed by the ocean (bottom) in W m^{-2}.

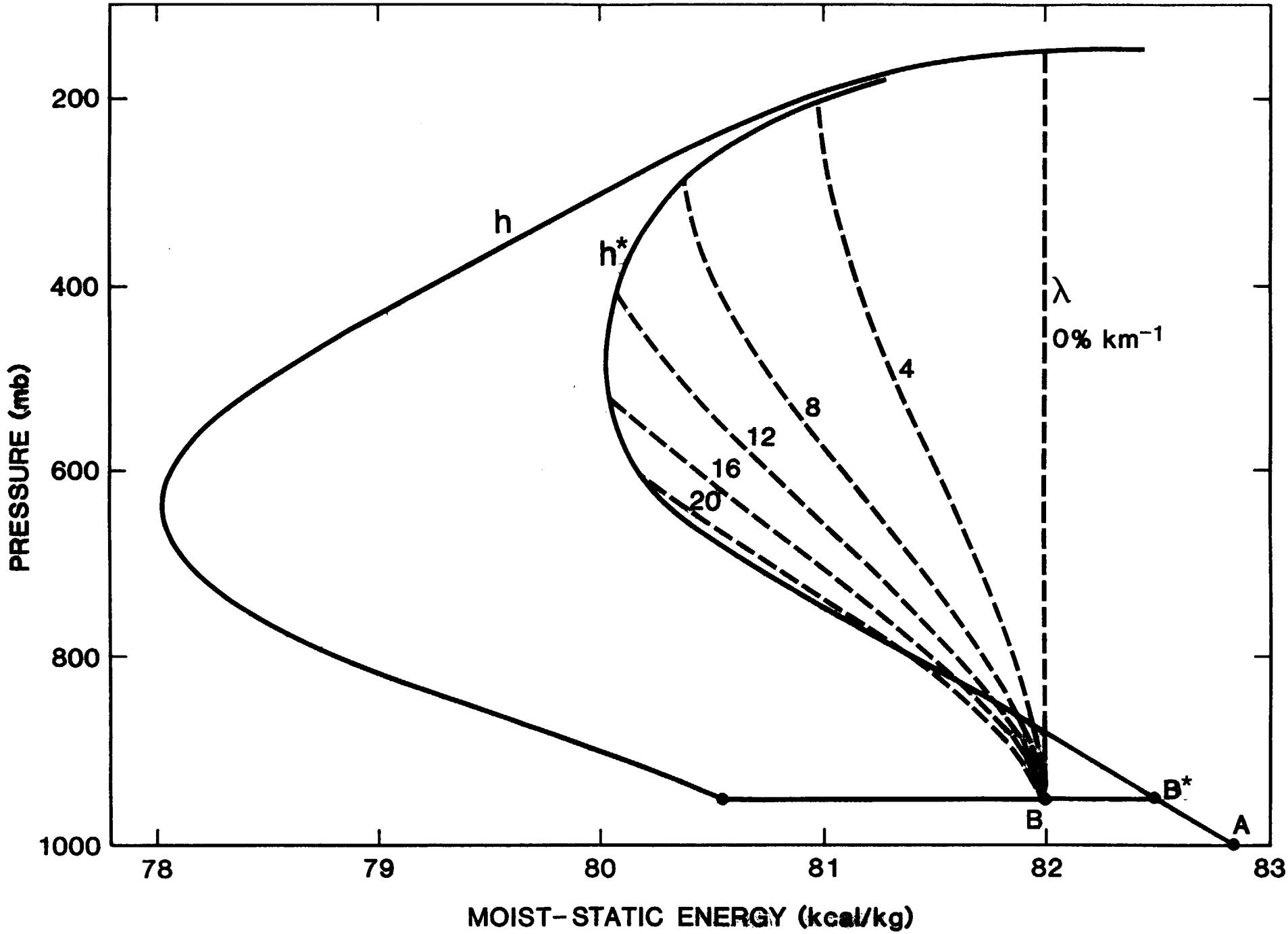
200
400
600
800
1000
PRESSURE (mb)
78
79
80
81
82
83
MOIST-STATIC ENERGY (kcal/kg)
h
h*
λ
0% km⁻¹
4
8
12
16
20
B
B*
A

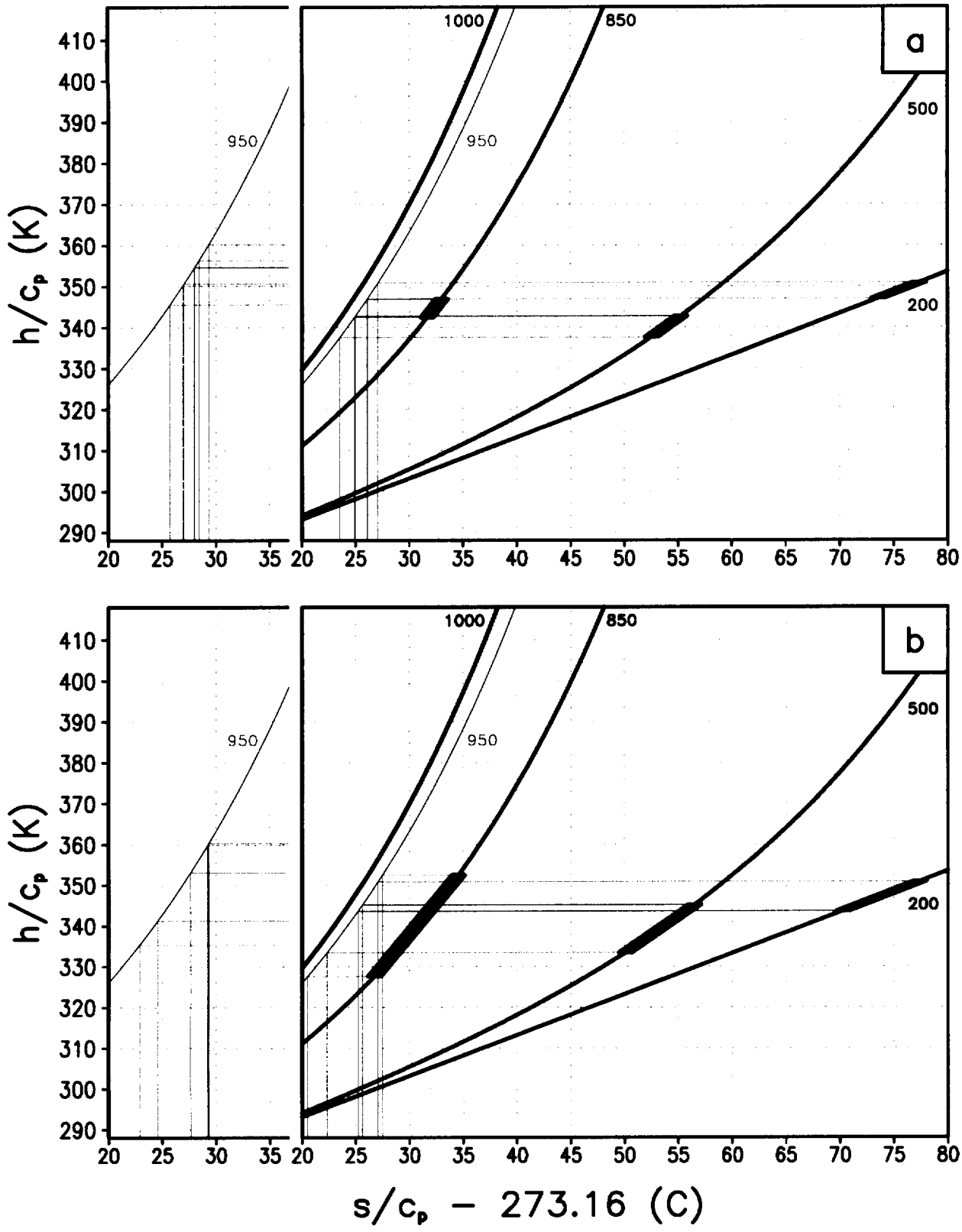

Fig 2. A complex plot showing (i) four lines for saturation moist static energy (h/c_p, in K) versus potential temperature (S/c_p, in °C); (ii) one line for cloud base moist static energy assuming 90% RH and 950 hPa pressure; (iii) riders for observed S/c_p with ±2 standard deviations of S/c_p; and (iv) left panels with CCWF+Δh_{ABL} corrections to h* (see text). Top (bottom) panels represent calculations for TOGA–COARE (ECMWF 1989) analysis of daily data.

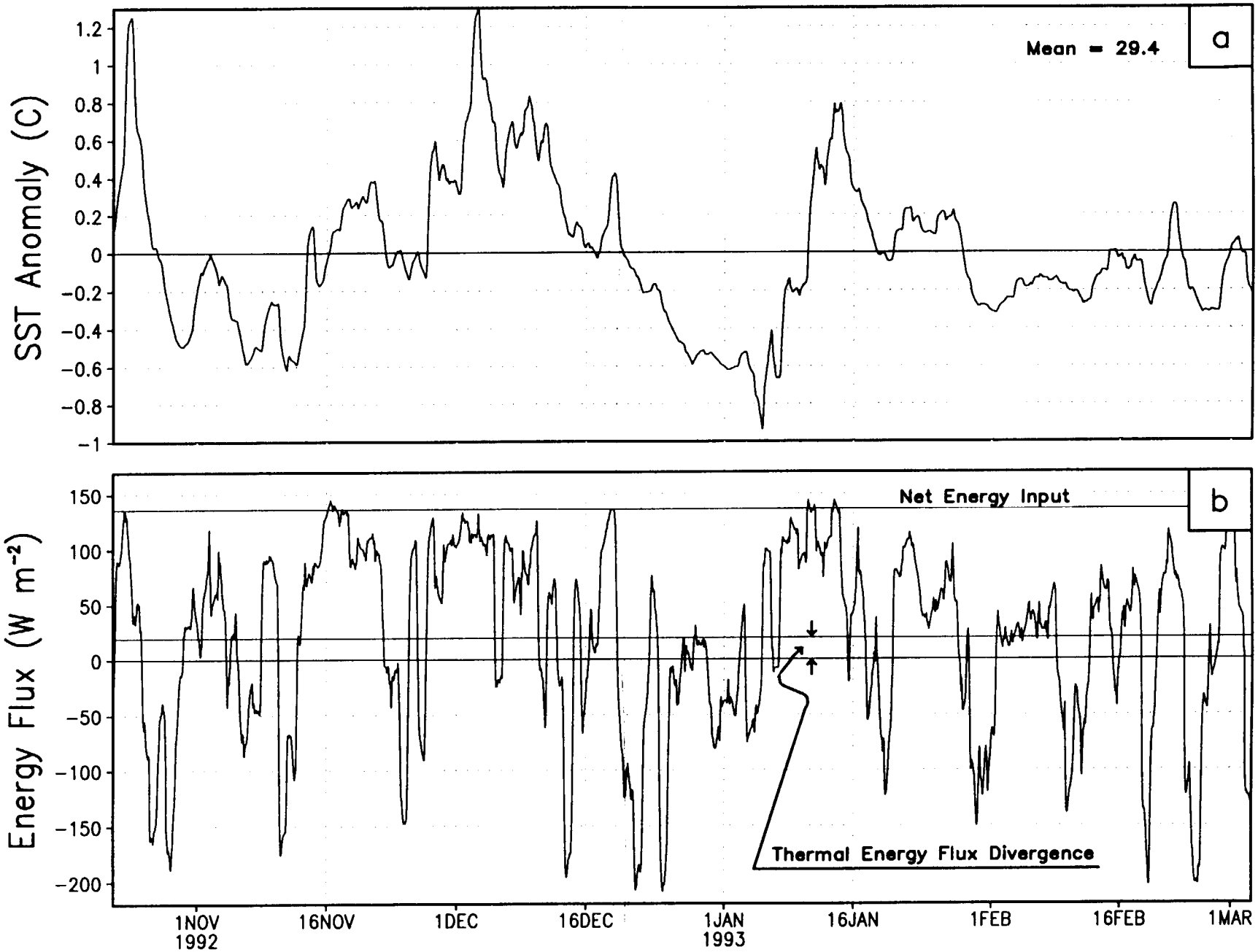

Fig 3. For the IMET buoy data collected in the TOGA–COARE IOP periods, 24h running means of (a) SST (°C) anomalies and (b) net energy fluxes into the ocean (W m^{-2}).

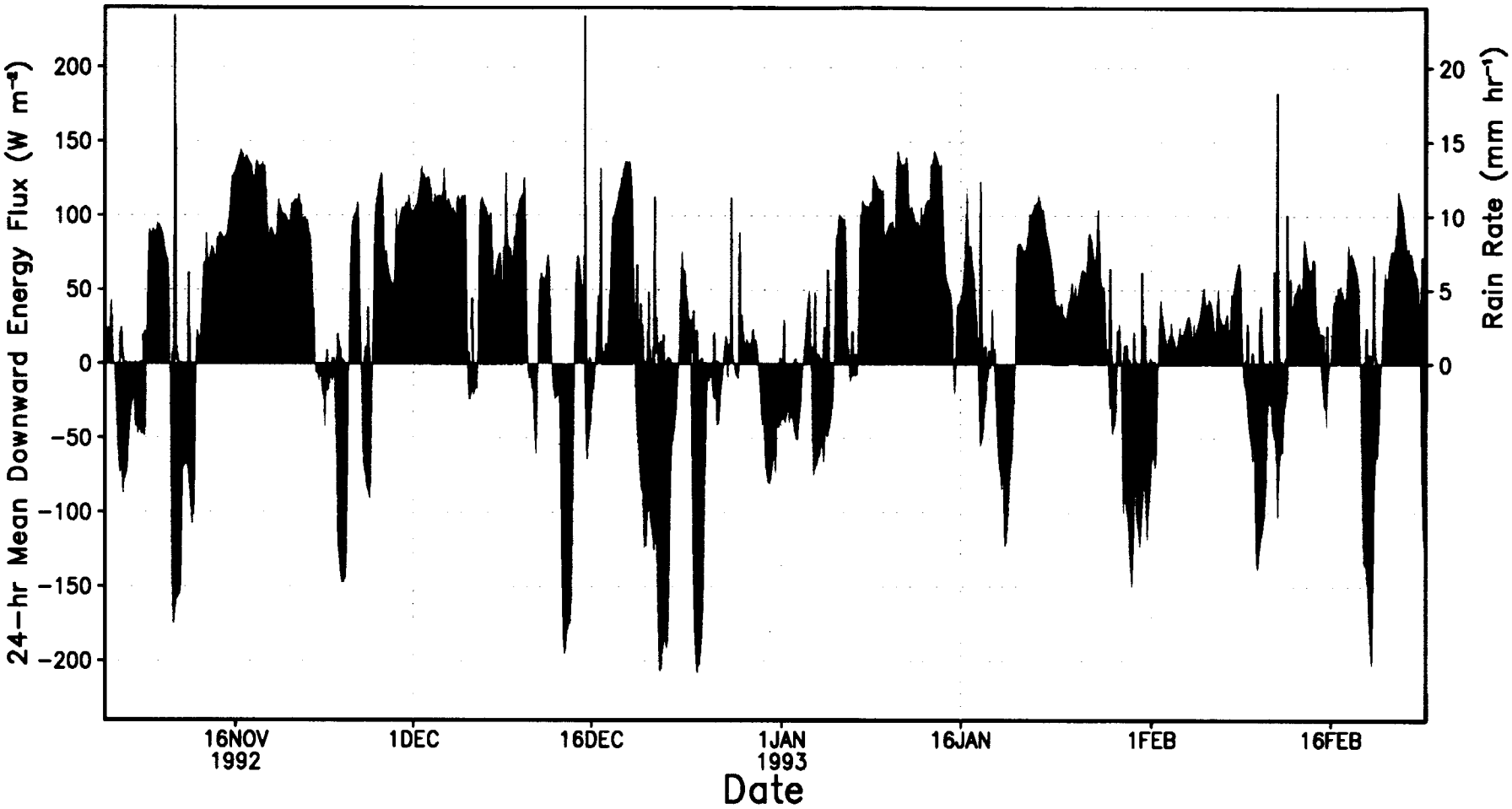

Fig 4. A composite plot of hourly precipitation (green) in mm h^{-1} and 24h running mean of downward energy flux (W m^{-2}) with red (blue) shades for positive (negative) values.

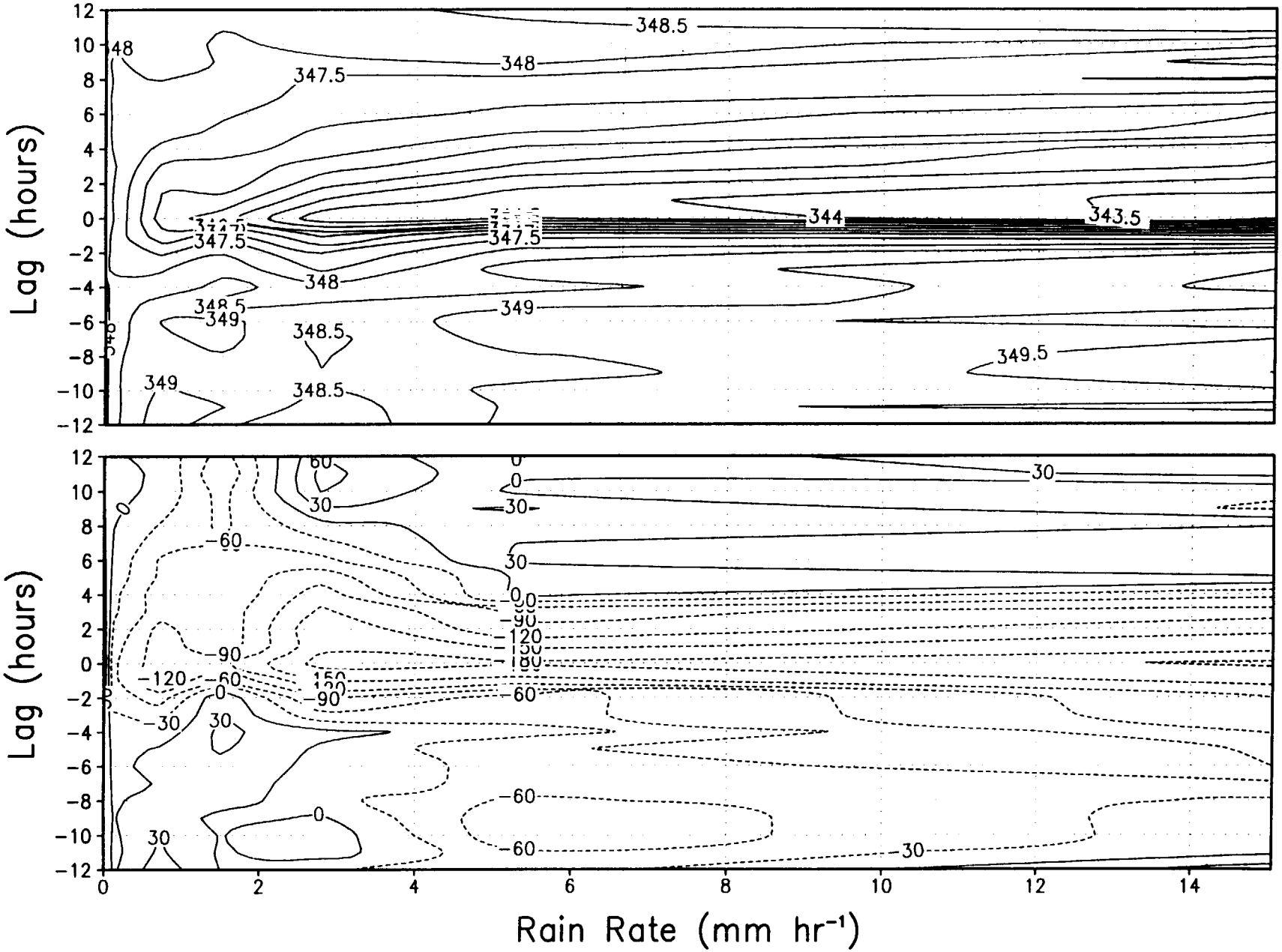

Fig 5. Moist static energy in kJ kg^{-1} (top) and net thermal forcing of the ocean (W m^{-2}) (bottom). The data was binned into equal sample sizes while lag or lead were used to collocate values at the same locations.

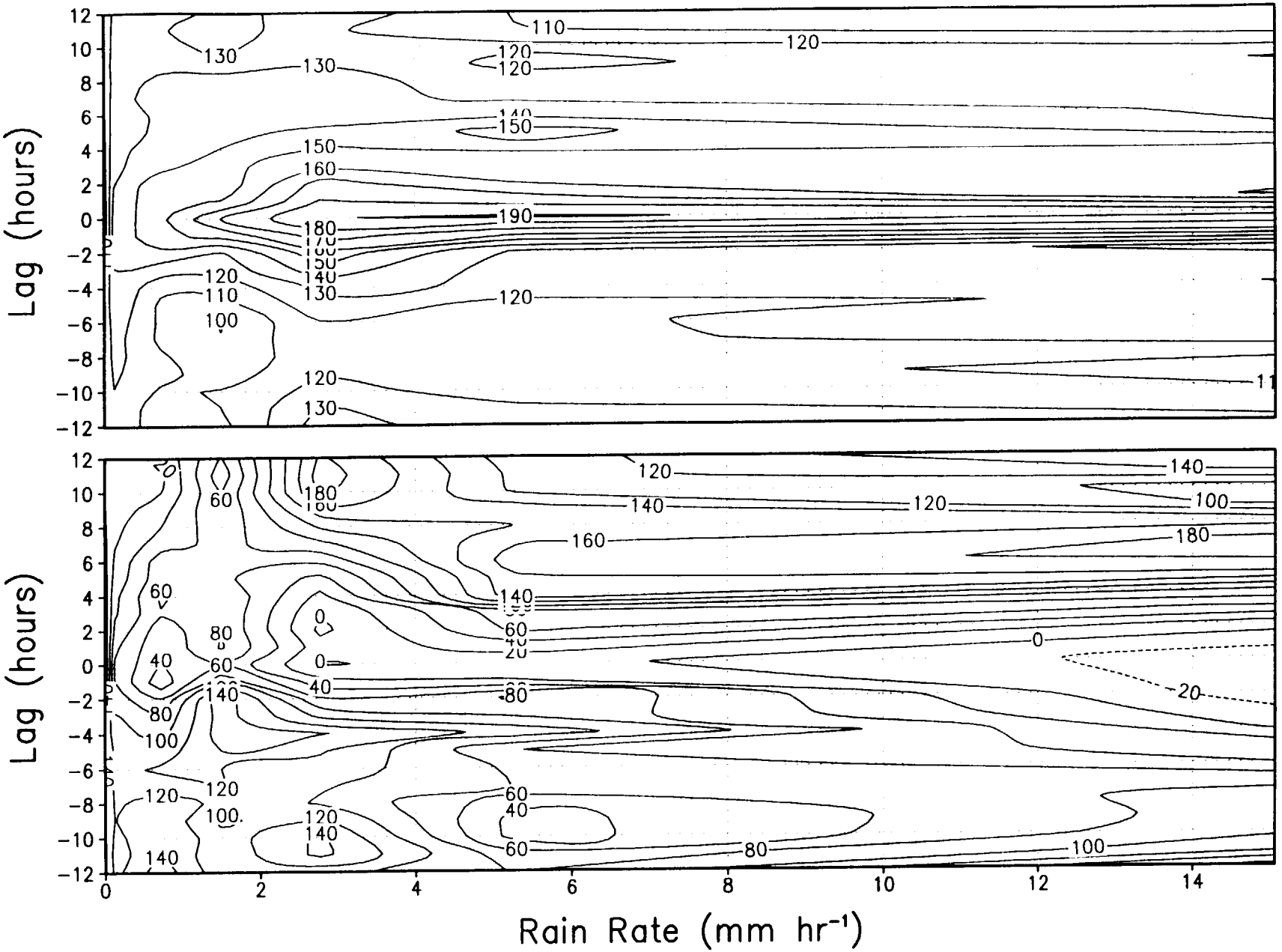

Fig 6. Same as Figure 5 except for latent plus sensible fluxes (top) and net radiation absorbed by the ocean (bottom) in W m^{-2}.